International Journal of Science and Technology (IJST)
ISSN: 3049-1118, Volume- 3, Issue- 2 (April - June 2026)

Diffusion Controlled Entirely Detached Growth of $in_{0.5}Ga_{0.5}Sb$ by VDS Process: Role of Interface Stability, Thermodiffusion, and Quasi-Microgravity Condition

Dattatray Gadkari
Independent Researcher

Abstract:

This study reports, for the first time, the diffusion-controlled growth of $In_{0.5}Ga_{0.5}Sb$ crystals under entirely detached conditions using the Vertical Directional Solidification (VDS) process in a vacuum-sealed quartz ampoule. The detached configuration eliminates crystal–wall contact, suppresses buoyancy-driven convection, and establishes a quasi-microgravity environment governed by diffusion and thermodiffusion. Crystal growth was achieved under controlled conditions of gap width (70–250μm), axial temperature gradient (10–32 °C·cm^{-1}), and translation rate (≤ 3 mm·h^{-1}), ensuring a stable and planar crystal–melt interface. Mass transport is governed by coupled Fickian diffusion and Soret-driven thermodiffusion, leading to systematic solute redistribution along the growth axis. A polarity transition from n-type to p-type conduction occurs near the equiatomic composition (~50% GaSb), confirming thermodiffusion-controlled segregation. Key transport parameters, including boundary layer thickness ($\delta \approx 0.05$–0.3 cm), diffusion time (~10^2 s), and a low Peclet number ($Pe \ll 1$), confirm diffusion-dominated growth with negligible convection. The constitutional supercooling criterion is satisfied under detached conditions, ensuring interface stability and defect-free solidification. Structural, electrical, and optical characterizations confirm high crystalline quality, reduced dislocation density, and excellent compositional uniformity. A dimensionless diffusion framework is introduced to quantify the transition from gravity-influenced to diffusion-dominated regimes. The results demonstrate that the VDS process enables quasi-equilibrium and quasi-microgravity solidification and provides a viable terrestrial alternative to alike microgravity-based crystal growth of high-quality $In_{0.5}Ga_{0.5}Sb$.

Keywords: $In_{0.5}Ga_{0.5}Sb$ detached growth; Vertical Directional Solidification (VDS); Thermodiffusion; Quasi-microgravity; Interface stability; Gravity–Diffusion number;

Introduction

Ternary III–V semiconductor alloys of the form $In_xGa_{1-x}Sb$ represent a technologically important class of materials due to their tunable bandgap, high carrier mobility, and strong infrared response, making them suitable for infrared detectors, thermophotovoltaic systems, and high-speed electronic devices [1]. Among these, the equiatomic composition $In_{0.5}Ga_{0.5}Sb$ is particularly attractive due to its ability to provide bandgap engineering across the mid- to

*Corresponding Author Email: db.gadkari@gmail.com
Published: 05 May 2026
DOI: https://doi.org/10.70558/IJST.2026.v3.i2.241251

long-wavelength infrared region. However, the growth of high-quality $In_xGa_{1-x}Sb$ crystals under terrestrial conditions remains a significant challenge. Conventional growth processes are strongly influenced by buoyancy-driven convection, thermocapillary flow, and solutal segregation within the melt, which disturb the solute distribution at the crystal–melt interface and lead to compositional inhomogeneity and structural defects [2]. These convective instabilities significantly affect interface morphology and crystal quality in III–V alloy systems.

Microgravity-based crystal growth experiments have demonstrated that the suppression of convection leads to diffusion-dominated transport, resulting in improved interface stability and enhanced compositional uniformity [3–12]. Detached or contactless growth under such conditions produces nearly planar solidification fronts and superior crystalline quality. However, space-based experiments are costly and operationally constrained, limiting their applicability for routine crystal growth [13–17].

To overcome these limitations, terrestrial approaches have been developed to simulate quasi-equilibrium (quasi-microgravity) conditions by suppressing convection and promoting diffusion-controlled transport. One such approach is diffusion-controlled solidification, which has been investigated as an alternative pathway for achieving high-quality crystal growth under controlled thermal conditions [18–20]. Previous experimental and theoretical studies have demonstrated that diffusion-dominated transport can significantly improve compositional uniformity and interface stability in semiconductor systems [21–29].

In diffusion-controlled systems, mass transport is governed by Fickian diffusion and thermodiffusion (Soret effect), where species redistribution occurs in response to temperature gradients rather than convective flow [30–35]. The stability of the crystal–melt interface is a critical factor in such processes and is governed by the Mullins–Sekerka stability criterion, which defines the conditions required to maintain a planar interface during solidification [36]. The Vertical Directional Solidification (VDS) process has emerged as an effective technique for achieving quasi-equilibrium (quasi-equilibrium) growth conditions under terrestrial gravity by controlling thermal gradients, growth velocity, and system geometry [37–51]. A unique feature of the VDS process is the possibility of achieving entirely detached growth, in which the crystal is separated from the ampoule wall by a narrow gap. This detachment eliminates wall-induced convection and lateral heat losses, thereby promoting diffusion-dominated transport and interface stabilization. Despite extensive studies on binary systems such as InSb and GaSb [21–29], the combined effects of thermodiffusion, interface stability, and quasi-equilibrium (quasi-microgravity) behavior in ternary In–Ga–Sb systems remain insufficiently understood. In particular, the conditions required to achieve stable, diffusion-controlled, entirely detached growth in $In_{0.5}Ga_{0.5}Sb$ have not been systematically established.

In this work, we report the diffusion-controlled, entirely detached growth of $In_{0.5}Ga_{0.5}Sb$ crystals using the VDS process under terrestrial conditions. The objectives of this study are: (i) to achieve a stable and planar crystal–melt interface under detached growth conditions, (ii) to investigate solute redistribution governed by thermodiffusion along the growth axis, (iii) to establish quasi-equilibrium solidification through suppression of convection, and (iv) to introduce a diffusion-based framework that quantifies the transition from gravity-

influenced to diffusion-dominated growth. The present study provides new insights into diffusion–thermodiffusion-controlled crystal growth and demonstrates that the VDS process offers a viable terrestrial alternative to microgravity-based crystal growth for ternary semiconductor systems.

2. Experimental Procedure

2.1 The preliminary growth requirements for VDS growth

High-purity elemental indium (In), gallium (Ga), and antimony (Sb) (purity ≥ 99.999%) were used as starting materials for the growth of $In_{0.5}Ga_{0.5}Sb$ crystals. The elements were weighed in stoichiometric proportions according to the composition listed in Table 1. The weighed materials were loaded into high-purity quartz ampoules with an inner diameter of 10–24 mm and a length of 100–140 mm. The ampoules were thoroughly cleaned, evacuated to a vacuum level of approximately 1×10^{-3} Pa, and subsequently sealed using an oxy-hydrogen flame. To ensure uniform melting and minimize contamination, the sealed ampoules were inspected for leakage and structural integrity prior to the growth process Non-linear axial temperature gradient of the vertical furnace was calibrated between 10–32°C.cm^{-1}, providing a controlled heat field. The translation velocity (V) was optimized [18–20, 37-51] to V ≤ 3mm.h^{-1}. More than eighty binary, doped derivatise and ternaries entire detached Sb-based crystals alloys had been successfully grown since 1994.

2.2 VDS Growth Configuration and Thermal Profile

Crystal growth ($In_{0.5}Ga_{0.5}Sb$) was carried out using a vertical directional solidification (VDS) furnace with a controlled axial temperature gradient figure-1. The furnace was calibrated to establish a non-linear axial temperature gradient in the range of 10–32 °C·cm^{-1}.

During growth, the central region of the furnace was maintained at approximately 850 °C (hot zone), while the lower region was stabilized near 500 °C (cold zone), thereby establishing a well-defined thermal gradient along the ampoule length figure 1b. The as detached ingot free movement is shown in figure 1c, and schematic the composition distribution is represented in figure 1d.

The translation velocity of the ampoule was maintained at ≤ 3 mm·h^{-1} to suppress convective flow and promote diffusion-controlled transport within the melt.

A programmed multi-step thermal cycle was employed to achieve controlled solidification figure 2a, b.

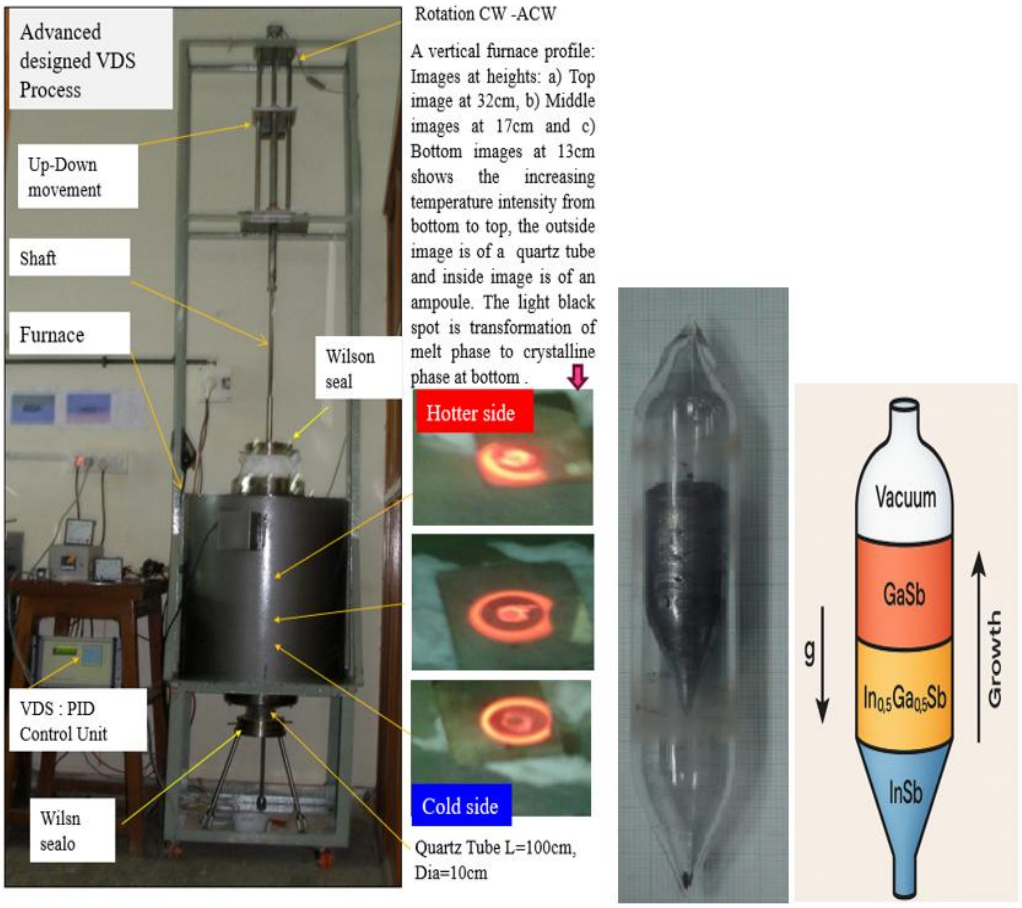

a **b** **c** **d**

Figure-1, a) VDS process photograph, b) the thermal images, c) detached ingot, d) Schematic growth

Table-1 Stoichiometric source materials for the growth of $In_{0.5}Ga_{0.5}Sb$ (IGS)

Elements	**IGS-1**	**IGS-2**	**IGS-3**	**IGS-4**	**IGS-5**	**IGS-6**	**IGS-7**	**IGS-8**	**IGS-9**
In	5.4955	5.1135	5.3703	5.1695	4.9834	4.8127	5.0935	5.8127	5.3127
Ga	3.3929	3.1038	3.2977	3.1310	2.8929	2.9223	3.0838	3.2123	3.1223
Sb	11.7132	10.9518	11.4135	11.2143	11.4687	11.2071	11.1218	11.2071	11.2071
InGaSb	20.6016	19.2691	20.0815	19.4938	19.4355	18.9421	19.3064	20.2321	19.6421

Growth Procedure

Step I: Pre-growth calibration: The furnace temperature profile and ampoule translation path

were optimized using dummy ampoules to establish the solidification zones corresponding to InSb, $In_{0.5}Ga_{0.5}Sb$, and GaSb phases.

Step II: Melting and homogenization: The loaded ampoule was heated to 850 °C within approximately 3 h and held for 12 h with rotation (~10 rpm) to achieve complete melting and chemical homogeneity of the charge.

Step III: Thermal stabilization: The melt was cooled to approximately 50 °C above the melting point of GaSb (~765 °C) and held for 6 h to stabilize thermal conditions.

Step IV: Entirely detached growth stage: The ampoule was translated downward at a rate of ~3 $mm \cdot h^{-1}$ under a controlled axial temperature gradient (10–30 $°C \cdot cm^{-1}$). During this stage, solidification occurred progressively along the growth axis, forming InSb at the cold end, GaSb at the hot end, and $In_{0.5}Ga_{0.5}Sb$ in the intermediate region. The growth proceeded under entirely detached conditions, characterized by the formation of a narrow gap between the crystal and the ampoule wall.

Step V: Completion of solidification: After completion of growth, the ampoule was cooled below the melting point of InSb and held at ~425 °C for 12 h to relieve thermal stresses.

Step VI: Controlled cooling: The furnace temperature was gradually reduced to ~250 °C over a period of 3 h to ensure uniform cooling and avoid thermal shock.

Step VII: Extraction of ingot: After complete solidification and cooling, the ampoule was removed, and the detached ingot was extracted. The total growth duration varied between 100 and 140 h, depending on the experimental conditions.

Temperature control throughout the process was achieved using a PID-based feedback system to ensure stability and reproducibility of the thermal gradients.

2.3 Detached Growth Characteristics

During solidification, a continuous narrow gap (≈ 70–250 μm) was formed between the crystal and the inner wall of the ampoule due to shrinkage and vapor-pressure effects. This gap effectively eliminated mechanical contact and minimized lateral heat conduction.

The detached configuration suppressed wall-induced convection and promoted a diffusion-dominated growth environment. The resulting crystal exhibited a smooth surface, absence of growth striations, and uniform morphology along the growth axis.

2.4 Characterization Techniques

The grown $In_{0.5}Ga_{0.5}Sb$ ingots were sectioned both longitudinally and transversely using a low-speed diamond saw. The samples were polished to a mirror finish using progressively finer abrasives.

The structural, compositional, and physical properties of the crystals were characterized using the following techniques:

- **Scanning Electron Microscopy (SEM)**: Surface morphology analysis
- **Metallurgical Microscopy**: Evaluation of dislocation density and microstructure

- **Nomarski Interference Microscopy**: Interface imaging
- **X-ray Diffraction (XRD)**: Phase identification and crystallographic analysis
- **Laue Back-Reflection**: Determination of crystal orientation
- **Hall Effect Measurements**: Electrical transport properties (carrier concentration, mobility)
- **Raman Spectroscopy**: Vibrational properties
- **Fourier Transform Infrared Spectroscopy (FTIR)**: Optical and bandgap characterization
- **Infrared Transmission Measurements**: Optical transmission behavior
- **Vickers Microhardness Testing**: Mechanical properties

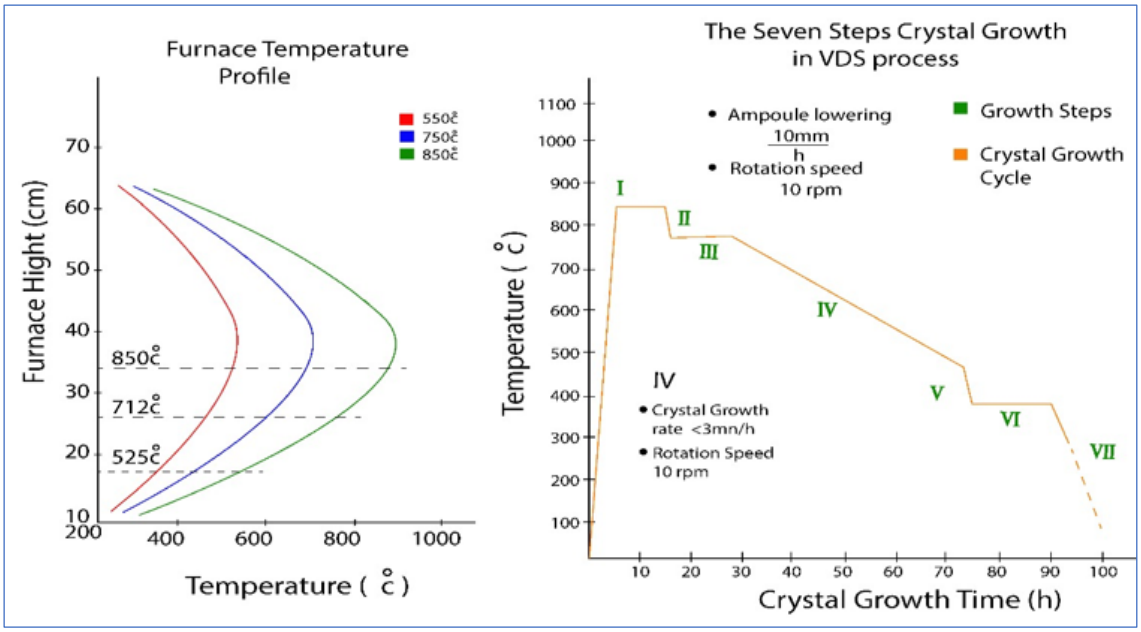

a **b**

Figure-2, a) the furnace temperature profile, and b) the typical seven steps crystal growth process

Results and discussion

3.1 Empirical Relation for Growth Dynamics

The growth behavior of $In_{0.5}Ga_{0.5}Sb$ under entirely detached conditions was analyzed using experimentally obtained data from multiple ingots. The growth duration was found to vary between 100 and 140 h, depending on the axial temperature gradient and ingot length.

An empirical relationship between growth time (T), temperature gradient ($G = dT/dz$), and ingot length (L) is expressed as:

$$\mathbf{T = (1/2.5) \cdot (dT/dZ) \cdot Lc + C} \quad (1)$$

where C is a constant incorporating the effects of cooling rate and translation velocity.

The agreement between calculated and experimental growth times confirms that the solidification process is primarily governed by thermal conditions and geometric parameters Table 2. This behavior is consistent with diffusion-controlled growth, where the interface kinetics are strongly coupled to the imposed temperature gradient.

Table-2 Calculation by the empirical formula for experimental and calculated ingot time period.

Sr number	Furnace height (cm)	Temperature (°C)	Ingot length L_C (cm)	Gradient dT/dZ (°C. cm^{-1})	Product (dT/dZ) x (Lc)	Expt. time T (h)	Calculated time T (h)
1	10	250	1	8	8	2.5	3.2
2	13	525	2	12	24	9	9.6
3	15	600	3	18	53	24	21
4	17	700	4	22	88	34	35.2
5	28	765	5	28	140	58	56
6	32	850	6	32	192	81	78.8

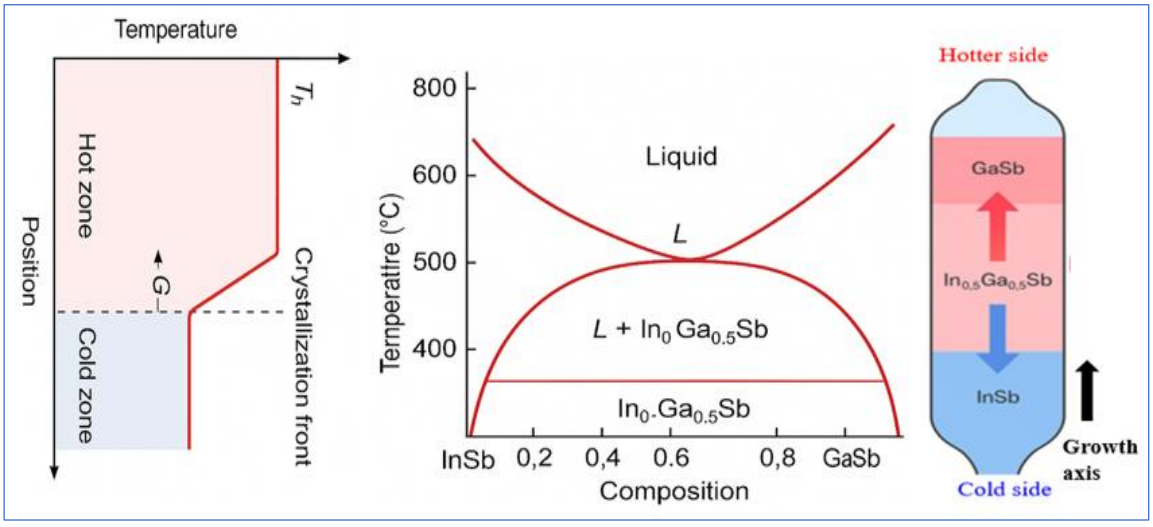

a **b** **c**

Figure-3, a) detached (shrinked at cold zone), b) composition variation, and c) binary and ternary phase

3.2 Morphological Evidence of Entirely Detached Growth

Macroscopic examination of the grown ingots provides direct evidence of entirely detached growth. The ingots were easily extracted from the ampoule without mechanical adhesion, indicating the absence of wall contact during solidification.

The following key observations confirm detached growth:

- A continuous and uniform gap (≈ 70–250 μm) between the crystal and ampoule wall
- Smooth surface morphology without striations or flow patterns
- Absence of growth bands and thermal-stress-induced cracks
- Uniform cylindrical geometry with a conical initiation region

The initial growth region exhibits a concave interface, followed by a planar interface in the middle region, and a convex interface toward the end growth stage. This transition reflects the evolution of thermal and solutal gradients along the growth axis.

The formation of the gap is attributed to shrinkage during solidification (figure 3a) combined with vapor pressure effects, which together create a self-sustained detached configuration. This configuration eliminates wall-induced heat transfer and suppresses convective flow, enabling diffusion-dominated growth.

3.3 Composition Evolution and Phase Redistribution

The compositional evolution along the growth axis demonstrates a clear redistribution of species driven by thermodiffusion figure-3b. At lower temperature gradients, the growth is dominated by In-rich composition corresponding to the InSb phase, whereas at higher gradients, Ga-rich composition corresponding to GaSb becomes dominant.

At approximately 50% GaSb composition, the system reaches a quasi-equilibrium state characterized by a planar interface and stable growth conditions. This composition represents the formation of the ternary $In_{0.5}Ga_{0.5}Sb$ phase.

The observed transition can be summarized as follows:

- Below 50% GaSb: In-rich region → concave interface → n-type conductivity
- At ~50% GaSb: balanced composition → planar interface → stable growth
- Above 50% GaSb: Ga-rich region → convex interface → p-type conductivity

This behavior confirms that the composition profile is strongly governed by the temperature gradient and associated thermodiffusion effects. The composition analysis is reported in Table-3.

In figure 3b, at GaSb % zero, the correspondingly the state is a binary InSb growth (concave interface and meniscus state), increase in temperature, the composition GaSb% also increases, thus, the ternary solidification phase of $In_{0.5}Ga_{0.5}Sb$ increases (L+ Solid $In_{0.5}Ga_{0.5}Sb$), simultaneously, Indium (In) concentration into solute decreases (L-line of liquid or melt), the growth is n-type $In_{0.5}Ga_{0.5}Sb$ semiconductor with increasing in concentration. This process continuous with increasing GaSb%, as the GaSb% composition nearing to 50%, the phase reversal impact as the further increase in temperature gradients, and at 50% GaSb composition, it is a state of equilibrium (planar interface and meniscus state). The phase reversal impact is after this state, here, the further increase in temperature gradients, and increase GaSb% composition the ternary phase of the $In_{0.5}Ga_{0.5}Sb$ solidification decreases (L+ Solid $In_{0.5}Ga_{0.5}Sb$), simultaneously, Gallium (Ga) concentration into solute increases (L-line of

liquid or melt). Growth is p-type $In_{0.5}Ga_{0.5}Sb$ semiconductor with decreasing in concentration. At GaSb % is 100, the ternary solidification phase of $In_{0.5}Ga_{0.5}Sb$ (L+ Solid $In_{0.5}Ga_{0.5}Sb$) is zero converting into binary phase of GaSb (convex interface and meniscus state). Therefore, the conclusion is that the GaSb% is 50%, the entire detached growth is planar interface state, the below 50%, the entire detached growth as concave interface, and above 50% the entire detached growth as convex interface figure-1c, and figure 3c.

This gap ensured uniform radial heat distribution and eliminated lateral conduction losses. It extended from the conical region, where, growth initiated upward against the gravity vector, the solid shrinks at crystallization front schematically as the detached growth figure-3a, the comparison of hot and cold zones. The GaSb % composition for respective temperatures is figure-3b, c. Here, 'G' is upward crystal growth (black arrow) as increased temperature gradient figure-3c, while V is the downward crystal translation velocity, and the cold zone at bottom and hot at top during growth process figure-1b, 3c. A measured continuous boundary layer (δ = 0.5-3mm) and a gap width (d = 70-250μm) with the inner wall of ampoule, figure-3a. The three phases indicate the regions of the InSb, $In_{0.5}Ga_{0.5}Sb$, and GaSb figure-3c, where transport is governed purely by diffusion.

Table-3 the composition analysis of six $In_{0.5}Ga_{0.5}Sb$ ingot grown by VDS process

Ele	IGS-1		IGS-2		IGS-3		IGS-4		IGS-5		IGS-6	
	Wt %	At%	Wt %	At%	Wt%	Wt %	At%	At%	Wt%	At%	Wt %	At%
In	18.1	14.5	18.7	17.1	17.80	17.4	15.8	17.9	18.42	16.86	17.6	15.8
Ga	30.7	44.3	29.2	40.3	28.66	29.4	41.6	38.6	29.42	40.61	29.4	41.6
Sb	51.1	41.0	52.0	42.5	53.54	52.0	42.5	43.4	52.06	42.52	52.8	42.5

(a)

Ele	IGS-1		IGS-2		IGS-3		IGS-4		IGS-5	
	Actual Wt	Comp %	Actual Wt	Comp %	Actual Wt	Comp %	Actual Wt	Comp %	Actual Wt	Comp %
In	5.396	18.13	5.114	18.72	4.170	18.42	5.370	17.80	4.170	18.42
Ga	3.293	30.70	3.104	29.26	2.531	29.42	3.298	28.66	2.531	29.42
Sb	11.610	51.17	10.952	52.02	8.844	52.06	11.414	53.54	8.844	52.06
IGS	20.299		19.269		15.545		20.082		15.545	

(b)

VDS configuration suppressed wall-induced convection, maintained uniform radial heat distribution (ΔT ≈ 1.4 °C), and promoted a diffusion-dominated process. The resulting ingots were easily released from the ampoule after cooling, confirming the grown crystal was contactless (no interface contact). The attached growth with convective forces figure-4a, while the planar surface structures condition for stability or reconstruction of interfaces during phase transformation, and interface stability evaluated the constitutional supercooling criterion figure-4b.

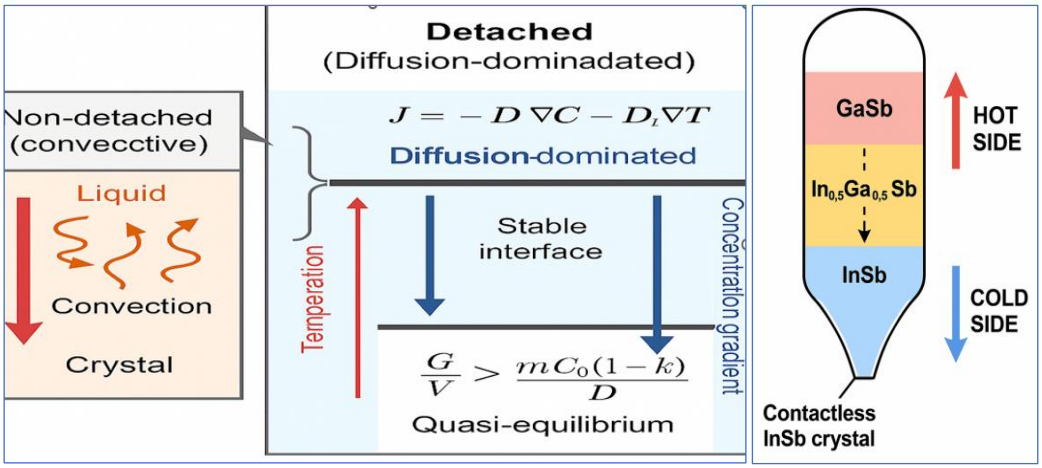

a **b** **c**

Figure-4, a) the attached growth, b) the entire detached growth, and c) The schematic contactless growth (white line in a conical blue region) and Soret redistribution of phases (InSb, $In_{0.5}Ga_{0.5}Sb$, GaSb) at hot and cold zones.

3.4 Interface Stability and Constitutional Supercooling

The stability of the crystal–melt interface is evaluated using the constitutional supercooling criterion:

$$G/V > m\,C_0\,(1 - k)/D \quad (2)$$

where G is the temperature gradient, V is the growth velocity, m is the liquidus slope, C_0 is the initial concentration, k is the partition coefficient, and D is the diffusion coefficient.

Under the present experimental conditions ($G \approx 32$ °C·cm^{-1}, $V \approx 3$ mm·h^{-1}), this criterion is satisfied, ensuring a stable planar interface figure 4b [30-36].

The absence of morphological instabilities, such as dendritic growth or cellular structures, confirms that the system operates within the stable regime. This stability is further supported by the lack of microsegregation and growth striations in the detached ingots.

This interface stability criterion for $In_{0.5}Ga_{0.5}Sb$ solidification under detached VDS conditions, the G–V (temperature-gradient versus growth-rate) diagram compares experimental data with the theoretical constitutional-supercooling boundary. Under detached conditions with G = 32 K.cm^{-1} and V = 3mm.h^{-1}, this criterion is satisfied, maintaining a planar interface and detached growth. The absence of striations and the microbands indicates uniform interface motion and minimal convective disturbance in VDS process figure- 4c, the red indicates the increasing

temperature gradients, which promotes redistribution of elements and concentration distribution along growth axis by thermodiffusion, thereby, the blue arrow in figure 4b, c indicated the cold zone with the detached or contactless ingot growth, a fine white line in conical region figure 4c, it enhanced crystallization into VDS process. The crystal–melt interface was detached as predicted from the ampoule wall owing to surface tension (capillarity effect) and vapor-pressure equilibrium. The blue arrow in figure- 4b was well within the planar region, whereas contact growth (downward red arrow) shows the convective perturbance figure-4a.

3.5 Diffusion and Thermodiffusion Mechanisms

Mass transport in the melt is governed by the combined effects of Fickian diffusion and thermodiffusion. The total solute flux (J) is expressed as:

$$\mathbf{J = -D\nabla C - D_T\nabla T} \quad (3)$$

where D is the mass diffusion coefficient and D_t is the thermal diffusion coefficient.

The ratio of these coefficients defines the Soret coefficient:

$$\mathbf{S_T = D_T/D} \quad (4)$$

The experimental results reveal a transition in the Soret coefficient from positive to negative values along the growth axis. This transition corresponds to a reversal in solute transport direction:

- $\mathbf{S_t > 0}$: solute migrates toward the cold region (In-rich zone)
- $\mathbf{S_t \approx 0}$: equilibrium state near 50% composition
- $\mathbf{S_t < 0}$: solute migrates toward the hot region (Ga-rich zone)

This thermodiffusion-driven redistribution plays a crucial role in stabilizing the composition and maintaining a uniform growth front.

For the validity of eqn-3, 4, the interface must planar and stable, the solute flux is under thermodiffusion, the growth obeys quasi-equilibrium (quasi-microgravity) environment. This is conceivable only when the crystal growth is under entire detached growth, which is plausible only by VDS process in terrestrial condition. The diffusion coefficient establishing a steady composition field under diffusion control, the boundary layer ($\delta \approx$ 0.5-3mm dark blue line figure-4b), where transport is governed purely by diffusion interface, ensuring interface stability and the steady adjacent meniscus gap ($d \approx$ 70-250µm) figure-3, 4. The equations for the growth velocity showed in a thick layer downward blue arrows figure 4b, growth velocity is independent of the thickness and is controlled by diffusion, whereas in a very thin layer, the growth rate is kinetic-limited on the interface [36].

3.6 Dimensionless Analysis of Transport Regime

To confirm the dominance of diffusion over convection, relevant dimensionless numbers were evaluated:

- **Peclet number (Pe)**: $Pe=vL/D \ll 1$

- **Rayleigh number (Ra)**: Ra~10^6

The low Peclet number indicates that advective transport is negligible compared to diffusion. The controlled Rayleigh number, combined with the detached configuration, suppresses buoyancy-driven convection.

As a result, the transport process is diffusion-dominated, closely resembling quasi-microgravity conditions.

3.7 Structural and Physical Characterization

XRD Analysis: X-ray diffraction confirms the formation of a single-phase zinc-blende structure with strong (220) orientation. The narrow full-width at half-maximum (FWHM) values indicate high crystalline quality and low defect density, Table-4.

FTIR Analysis: FTIR measurements show a gradual increase in bandgap energy from ~0.16 eV (InSb) to ~0.71 eV (GaSb), consistent with compositional variation along the growth axis.

Raman Spectroscopy: Raman spectra exhibit characteristic transverse optical (TO) and longitudinal optical (LO) phonon modes, confirming crystal structure and phase purity.

Hall Measurements: Electrical measurements reveal a transition from n-type to p-type conductivity near the equiatomic composition, consistent with thermodiffusion-driven segregation.

Microhardness: Vickers microhardness values indicate improved mechanical strength and reduced dislocation density compared to conventionally grown crystals

The composition measurements

For the composition % of $In_{0.5}Ga_{0.5}Sb$ samples were selected from the central part of each detached crystal. A composition (%) measured after the conical shape and before the convex shape Table 3a, b - a) composition % and b) measured weight composition%. The weight of elements and their atomic weight represent the elements actual weight and their corresponding composition % along ingot length. The composition % of six entire detached ingots by EDAX Table-3, while the changes in composition % along length 'x' of samples of IGS-1 to 6 was measured Table 3. The axial and transverse elements mol% per mm variation $\Delta x < 0.01$. This attributes that the thermodiffusion, planar interface and quasi-equilibrium conditions were contributed contemporaneously (synchronously) in the entire detached growth into the controlled VDS growth process.

Table-4 XRD data of entire detached $In_{0.5}Ga_{0.5}Sb$ crystals grown by VDS process

IGS1-12		IGS2-13		IGS3-11		IGS4-11		IGS5-10		IGS6-11	
2θ	d	2θ	d	2θ	d	2θ	d	2θ	d	2θ	d
24.27	3.705	25.289	3.520	25.18	3.534	23.76	3.742	24.96	3.564	24.12	3.705
39.70	***2.228***	***41.66***	***2.146***	***38.9***	***2.23***	***39.36***	***2.287***	***41.5***	***2.13***	***39.7***	***2.22***

				0	***4***			***2***	***9***		***7***
46.90	1.936	49.55	1.838	41.46	2.176	46.50	1.951	41.62	2.168	46.9	1.936
57.14	1.64	60.72	1.524	49.32	1.846	71.32	1.321	49.22	1.85	57.14	1.64
62.84	1.478	66.81	1.399	60.42	1.531	71.68	1.316	49.40	1.84	62.84	1.478
63.08	1.477	76.51	1.244	66.52	1.404	76.40	1.246	60.28	1.534	63.08	1.477
71.72	1.315			76.06	1.25			65.72	1.42	71.72	1.315
76.94	1.238							75.74	1.255	76.94	1.238

3.7.1 XRD measurements

For XRD measurements, the substrates samples were selected from an entire detached $In_{0.5}Ga_{0..5}Sb$ ingot middle section. The italic black numbers Table 4 are the preferred (220) reflection of diffraction, was attributed to the growth direction at 2θ, and the (110) orientation of as grown ingots with the maximum I/I_0 peak intensity ratio. These sharp peaks values for (220) diffraction were compared with the ASTM/ JCPDS, CuKα λ=1.5405A^0, the card numbers are -- i) **InSb** card number 6-208: a = 6.4782A^0, d = 2.290, hkl = 220, 2θ = 39.9098, ii) **GaSb** card number 7-215: d = 2.156, hkl = 220, 2θ = 41.8639. However, the values of InSb and GaSb of the six $In_{0.5}Ga_{0..5}Sb$ detached ingots are reported Table-4, which reveals that the 2θ decreases, it indicates the blue shift towards lower values. Table 3 and 4 contribute the high-composition quality crystal growth. The experimental and numerical simulations [21-29] confirms that the VDS growths were diffusion-controlled growth process. X-ray diffraction also confirmed a single-phase zinc-blende structure of $In_{0.5}Ga_{0.5}Sb$ without secondary phases. The full width at half maximum (FWHM) of the (220) reflection was < 100 arcsec, indicating high crystalline perfection. Etch-pit density (EPD) values ranged from 1.4 × 10³ to 5.3 × 10³ cm^{-2}, nearly an order of magnitude lower than growth of contact with ampoule inner wall (2–3×10⁴cm^{-2}). Further, Vickers hardness (H_v = 3.7 GPa) corroborates reduced defect density [49-51]. These data confirms that the enhancement of crystallization by the thermodiffusion, planar interface and quasi-equilibrium condition, which was contemporaneously existed during the entire detached growth of the $In_{0.5}Ga_{0.5}Sb$ crystals into VDS process, hence, corroborates enhanced crystallization of the $In_{0.5}Ga_{0.5}Sb$ into VDS.

3.7.2 FTIR measurements

FTIR measurements Table-5 reveals how the entire $In_{0.5}Ga_{0.5}Sb$-1 (IGS) detached growth process into VDS was transpired. The wavenumbers and wavelengths were measured along growth axis; the measured energy gap reveals that the energy gap increases from a conical ingot

shape (0.16 eV for InSb) towards the end of growth (0.71eV for GaSb). While, the middle variation corresponds to the ternary $In_{0.5}Ga_{0.5}Sb$ energy gap was for species (In, Ga, Sb) redistribution according to the temperature gradient effect on concentration into solute solution melt, thus, the binary InSb - ternary $In_{0.5}Ga_{0.5}Sb$ - binary GaSb phases were established into solute solution by thermodiffusion. This indicates composition variation, because of species redistribution by temperature gradient which influenced the concentration variation in solute solution under stable and steady condition, and the smooth increase of energy is related to the heat and maas transfer by the thermodiffusion. It is attributed to the planar and steady state crystal-melt interface, it reveals the smooth increased thermal gradient, which influenced homogeneous concentration gradient near the solidification front by detached growth into VDS process. For perfect single binary crystals, the transmission % -- InSb (38%) and GaSb (34%), while the ternary $In_{0.5}Ga_{0.5}Sb$ detached ingots showed the low FTIR transmission % as compared to binary (InSb, GaSb) entire detached crystals. The n-type region, the band gap engineering varies from 0.15eV to 0.21eV, while, the p-type region, the band gap tailored from 0.3eV to 0.58eV, are potential for Infrared applications in electromagnetic spectrum as shown in Table5. Further, the increasing in energy gap concludes as the Indium concentration decreases (reported for Space grown crystals [21-29]) while Gallium concentration increases along ingot length as temperature gradients increases. It confirms the species transport towards cold (InSb) and hot (GaSb) zones, and the thermodiffusion, [30-35] the planar interface [36], and melt governing equations. [21-29]] into VDS process [37-51]. Therefore, the thermoduffusion, planar interface, quasi-microgravity and the melt governing equations processing were controlled in VDS process.

3.7.3 Raman spectroscopy

Raman spectroscopy of $In_{0.5}Ga_{0.5}Sb$, n-type semiconductor properties of $In_{0.5}Ga_{0.5}Sb$-1 below 50% composition showed the prominent sharp peak at 181.7cm^{-1}modes was υTO (Γ) modes and the low peak at 192cm^{-1} was υLO (Γ) modes. However, $In_{0.5}Ga_{0.5}Sb$-1ingot growth after 50% composition showed

Table: 5 FTIR measurements, smooth parameters variation into VDS grown $In_{0.5}Ga_{0.5}Sb$ crystals

Sr No.	Sample No.	Wave number	Wavelength (μm)	Energy Gap (E_g eV)	IR range Application
1	InSb	1391	7.75μm	0.16eV	LWIR ~7-14 μm
2	IGS1-2	1427	7.0077	0.1769	
3	IGS1-4	1507	6.6357	0.1862	
4	IGS1-5	1521	6.5746	0.1886	
5	IGS1-6	1545	6.4725	0.1916	
6	IGS1-8	1663	6.0132	0.2062	

7	IGS1-10	1695	5.8997	0.2102	MWIR~3-6 µm
8	IGS1-11	2042	4.8972	0.2532	
9	IGS1-13	2389	4.1684	0.2974	
10	IGS1-15	2736	3.6550	0.3393	
11	IGS1-18	3447	2.9010	0.4274	SWIR ~1-3µm
12	IGS1-20	3815	2.6210	0.4731	NIR 0 .75-1 µm
13	IGS1-22	4707	2.1243	0.5837	

the p-type semiconductor properties of the prominent sharp peak at 210 cm^{-1} were υTO (Γ) modes, and the low peak at 178 cm^{-1} was υLO (Γ) modes. First prominent vibration mode of sharp peak reveals the

crystallization direction (220) of the ingots, the second minor weak peak attributes the low defect density (< 10^3 cm^2). Raman shift was interaction between bonds of similar energies in a molecule, lead to a spectrum shift different by molecules vibrations. Raman spectra of binary InSb and GaSb has the sharp peak at 174.2 cm-1 and 221.65cm-1 respectively, whereas, the ternary $In_{0.5}Ga_{0.5}Sb$ was within these ranges, was identified as υTO (Γ) modes and the anti-stokes zincblende structure. Only TO phonon showed the (220) backscattering direction. It shows the single orientation growth. The perfect crystals growths due to entire detached growth of the $In_{0.5}Ga_{0.5}Sb$ crystals by diffusion and interface stability controlled VDS process.

3.7.4 Vickers Microhardness test:

The indentations of six $In_{0.5}Ga_{0.5}Sb$ crystals are IGS-1 = 2.19GPa, IGS-2 = 2.87GPa, IGS-3 = 3.02GPa, IGS-4 = 3.72GPa, IGS-5 = 3.85GPa, and IGS-6 =3.98 GPa. The binary InSb and GaSb, Hv = 2.21GPa and Hv= 4.42 GPa respectively. The higher values of hardness were attributed to enhanced crystallization attributed of the entire detached ingots, and the lower dislocation density. Conclusion from these measurements, the extremely high order strength of the perfect single crystallization grown by entire detached growth into VDS process, which confirmed that d < 10^3cm^2 due to the breaking of covalent bonds of atoms to increasing hardness. On the other hand, the perfect crystals hardness, where, dislocation range 10^3cm^2 to 10^4cm^2 was dislocation-dislocation motion. Whereas, the low-quality crystals have dislocation range >10^4cm^2, the hardness decreases with increase in dislocation density, then, the motion of dislocations energy > 10^5cm^2. This proved successful entire detached growth by the diffusion and interface stability into controlled VDS process.

3.7.5 Electrical transport (Hall Measurements)

Hall-van der Pauw electrical parameters of $In_{0.5}Ga_{0.5}Sb$ are in figure 5, in this graph the GaSb% composition along growth axis, which also corresponds to figure 3b. These are from respective ten growths, the overall measurements conclusions are - i) the n-type growth (up to 50% of GaSb% composition), mobility decreases from $1.6\times10^4cm^2$ $V^{-1}.s^{-1}$ to $712cm^2$ $V^{-1}.s^{-1}$

representing the red line in figure 5 (L-line melt phase figure 3b), which was indicating the Indium concentration into melt decreases. While the carrier concentration increases from 2.4×10^{16} to 8.6×10^{18} cm^{-3}, green line figure 5 (the L + $In_{0.5}Ga_{0.5}Sb$ solidification phase) representing the significant growth by increasing GaSb% composition up to 50% in figure 3b, 5. Interesting behaviour of the phase reversal beyond 50%, the GaSb% composition increases showing the p-type growth, mobility increases from 7×10^{2} to 1.2×10^{3} $cm^2.V^{-1}$ s^{-1} red line in figure 5 (L-line melt phase of Ga increases figure 3b), while, the solidification phase showed the carrier concentration decreases from 8.6×10^{18} to 2.7×10^{17} cm^{-3} green line figure 5. It shows the ternary $In_{0.5}Ga_{0.5}Sb$ phase converted into binary GaSb phase at 100% GaSb composition.

However, the resistivity varies from 2.98×10^{-4} to 3.6×10^{-2} Ω·cm, and the band gap increases in the range of 0.16 eV (InSb) to ~0.71×eV (GaSb) Table 5, confirming enhanced compositional uniformity and crystal quality improvement. The measurements confirmed that the detached crystal growth rate averaged 2.5 $mm.h^{-1}$, nearly twenty times higher than for InGaSb crystals rates reported for space-grown (0.016 $cm.h^{-1}$) or Earth-based (0.011–0.012 $cm.h^{-1}$) [21–29]. The hall measurement performance confirms the thermodiffusion effect of species redistribution (Soret effect) by controlled solute redistributions as well as the resulting electrical compensation mechanism in ternary detached $In_{0.5}Ga_{0.5}Sb$ crystals. The redistribution and stabilizing the crystal–melt interface, suppresses constitutional supercooling, and enhances kinetic smoothness, yielding improved crystal quality compared to conventional growth methods. The compositional variation in figure 3b and the corresponding carrier-concentration profile in figure 5 exhibit a strong correlation, reproducing the compositional evolution of the $In_{0.5}Ga_{0.5}Sb$ entire detached growth. It is attributed to the transport of elements during the entire detached growth, [37-51] and the contemporaneously thermodiffusion [30-35] planar interface [36], and melt governing equations [21-29].

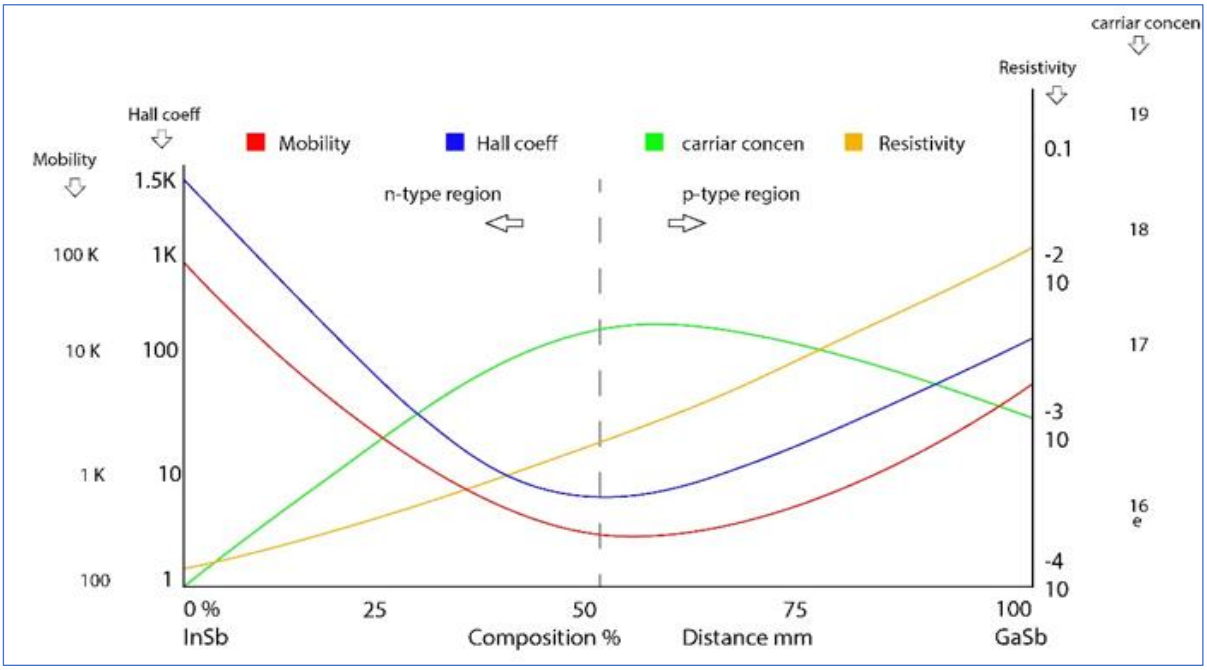

Figure-5 Hall-van der Pauw electro-physical measurements of $In_{0.5}Ga_{0.5}Sb$ shows the mobility, carrier concentration, resistivity, and Hall coefficient

3.7.6 Dimensionless transport analysis

The effectiveness of diffusion controlled VDS configuration is confirmed in 3.3.1 to 3.3.6, then, envisaged that the VDS process effectively reduces gravitational convections by contactless growths (a quasi-microgravity ~10^{-3}–10^{-4} g-equivalent) at crystal-melt interface (solidification) front. The entire detached gap width grown by the surface tension effect and the vapour-gas pressure, thus the crystal-melt interface and meniscus, which was measured, and it showed conjured the $In_{0.5}Ga_{0.5}Sb$ crystal growth. To strengthen it, the dimensionless number effect in diffusion-dominated transport is evaluated for confirmation, were calculated using the values Table 8. Dimensionless numbers were evaluated for convection suppression; these numbers values are below –

I). Rayleigh number **Ra** = $g\beta\Delta TL^3/(\nu\alpha) = 4.2x10^6$

normal range rang (10^6 to 10^8), no fluid motion and heat transfer is only diffusion than convection.

II. Grashof number **Gr** = $g\beta\Delta TL^3/\nu^2 = 7.7x10^6$

III. Prandtl number **Pr** = $\nu / \alpha = 1$

IV. Rayleigh **Ra** = Gr × Pr = $7.7x10^6$, both heat and momentum diffuse at the same rate.

V. Peclet number **Pe** = $vL/D = 0.11$

VI Pe << 1, a diffusion dominant process, convection was strongly suppressed; the transport occurred mainly by heat and mass transfer, figure 4b.

The estimated Rayleigh number (Ra) confirm that both buoyant and surface-tension–driven flows are negligible in the detached growth by VDS process. Accordingly, the interface stability was dominated by the coupled diffusive and thermodiffusive fluxes predicted by Fick's (diffusion) and thermodiffusion relations. Successively, the diffusive transport dominates over advective flow, the mechanical decoupling provided by the gap width prevents the buoyant convection. Effective gravity within the detached layer at crystal-melt interface state, estimated at 10^{-3}–10^{-4} g-equivalent at the solidification front. The diffusion-controlled growth achieved solely through ampoule detachment in VDS process and thermal stabilization, effectively reproduces the conditions comparable to solidification experiments in quasi-microgravity.

Table-6 Calculation of parameters involved in the $In_{0.5}Ga_{0.5}Sb$ entire detached growth by VDS process

Sr No.	Ingot length cm	Gradient dT/dZ °C.cm^{-1}	Growth velocity V cm/s	Concentra C (cm^{-3})	Diffusion Coeff D cm^2	Ther mo diffusion D_T m^2/s.C^{-1}	Soret Coeff. S_T
1	1	12	0.3	$4.2x10^{16}$	0.025	0.0021	0.0833
2	1.5	14	0.3	$7.3x10^{16}$	0.043	0.0023	0.0527

3	2	16	0.3	$1.2x10^{17}$	0.056	0.0034	0.0614
4	2.5	18	0.3	$4.1x10^{17}$	0.067	0.0026	0.0392
5	3	20	0.3	$5.2x10^{17}$	0.075	0.0041	0.0550
6	3.5	22	0.3	$5.9x10^{18}$	0.082	0.0026	0.0318
7	4	24	0.3	$6.2x10^{18}$	0.013	0.0125	0.0125
8	4.5	26	0.3	$3.2x10^{18}$	0.012	0.0588	-0.0186
9	5	28	0.3	2.7×10^{17}	0.011	0.0329	-0.0179
10	5.5	30	0.3	1.7×10^{17}	0.010	0.0001	-0.0124

3.7.7 Sore effect and composition evolution

Solidification concentration increases from binary InSb to ternary $In_{0.5}Ga_{0.5}Sb$ up to 50% composition along axis figure 3b, and the calculated parameters Table 6, 7. Because, the InSb moved to colder side positive sign ($S_T > 1$) due to thermodiffusion effect along ingot length by increasing concentration correspondingly increase in temperature gradients by Soret effect. Therefore, the Diffusion coefficient (D), the thermodiffusion (D_T), and the Soret coefficient (S_T), these parameters into VDS process increases, it validates the thermodiffusion phenomena. On the other hand, after 50% composition, the solidification concentration decreases from ternary $In_{0.5}Ga_{0.5}Sb$ to binary GaSb enrichment figure 3b, it indicates that $S_T < 1$ (negative) Gallium moved to hot zone. The parameters diffusion coefficient (D), the thermodiffusion (D_T), and the Soret coefficient (S_T) decreases into VDS process confirming the thermodiffusion phenomena. The entire detachment by VDS process, $In_{0.5}Ga_{0.5}Sb$ originates from the Soret-driven solute redistribution, and the quasi-equilibrium diffusion was established as the n-type to p-type transition. The concentration increases sharply with an increasing thermal gradient up to 23–24°C.cm^{-1}, showing enhanced atomic migration under higher thermal driving forces. Beyond this, the concentration begins to decreases, indicating a possible reduced thermal stability. The crystal quality revealed the Soret-driven effect impact promoted the superior crystallization reproducibility.

3.8 Thermodiffusion under quasi-microgravity conditions

The conical geometry of ampoule and the controlled crystal-melt interface movement, promotes the spontaneous detachment of oriented seed, which was a contactless $In_{0.5}Ga_{0.5}Sb$ solidification growth along axis. A narrow gap width was measured between the inner wall of an ampoule and the growing crystal, confirming entire detachment, which suppressed the wall-induced heat and the secondary growth of nucleation in $In_{0.5}Ga_{0.5}Sb$ detached growth in VDS process. The increased temperature gradients promote a steady-state concentration into the melt consistent with a diffusion-controlled process, as indicated by the calculated Soret coefficient values Table 6, 7. The dimensionless numbers in 3.3.7, indicate that the buoyant and surface-tension–driven flows are negligible. Accordingly, the solute redistribution occurs in a purely diffusive environment that is equivalent to quasi-equilibrium solidification condition. Hence,

detached growth in VDS process manifest a reproducible state for simulating solidification medium of low-gravity, and the thermo-diffusion dominated segregation phenomena. Calculated Soret coefficient (S_T), Table 6, exhibits a distinct evolution along the detached growth axis and the crystal-melt interface influence the In-rich dominate at cold side and the GaSb-rich near hot end Table 7. The polarity reversal at temperature 24°C was the transition from strong thermodiffusion to a quasi-equilibrium, in which, the gallium transport dominates at higher temperatures. The suppression of convective transport into detached growth VDS process allows diffusion and thermal gradients to act as the mass transport mechanisms throughout the melt. Subsequently, the solute redistribution occurs in a diffusion-controlled environment due to quasi-microgravity conditions. This confirms that the detached VDS process realizes diffusion-controlled crystal growth conditions analogues to quasi-microgravity environment. The diffusion coefficient was estimated using a simplified 1D steady-state approximation (neglecting convection and interface kinetics) Table 6, 7.

Table-7 Calculation of the Soret coefficient (S_T)

Stage	G(°C/cm)	D (cm^2/s)	ΔC (cm^{-3})	S_T	Remark
Zone-I	12	0.025 ↑	4.2×10^{16}	1.97	In-rich diffusion
Zone-II	15	0.035 ↑	8.7×10^{17}	5.32	In-minor diffusion
Zone-III	20	0.055 ↑	5.7×10^{18}	6.19	In-negligible diffusion
Zone-IV	24	0.013 ↓	6.2×10^{18}	−0.01	Reversal near equilibrium
Zone-V	30	0.011 ↓	1.7×10^{17}	~0	Diffusion nearly frozen

3.9 Quasi-Equilibrium Interface Stability in VDS process

In VDS process, the fine gap width acts as a natural thermal buffer figure 4c (fine white line in conical region), suppressing shear stress transfer and damping convection. Hence, even under 1g conditions, the system effectively behaves as alike quasi-microgravity, governed by diffusion and thermodiffusion dynamics figures 3-4. The attached gravity driven convection within figure 4a and the entire detached growth figure 4b, c. Sealed quartz ampoule exhibits a continuous a narrow gap width along its inner wall figure 4c, which promotes the mechanism of detachment and quasi-equilibrium-controlled growth, The upward temperature gradient (G) and downward translation velocity (V) induces counter-diffusive fluxes. The thermal gradient increase (G) induces Soret-driven thermodiffusion in the intermediate zone of the $In_{0.5}Ga_{0.5}Sb$ alloy (yellowish) under quasi-equilibrium diffusion control, it suppresses convection yielding a planar interface. The S_T variation demonstrates an exponential increase with temperature gradient Table 6, 7. This suggests stronger thermodiffusion effects driven by the temperature field at higher gradients. The increase in S_T reflects the enhanced coupling between heat and mass transport processes within the crystal melt during VDS process. Further, reveals three distinct phases, at low gradients (below ~20 $K.cm^{-1}$), is positive S_T >1, indicating reverse thermodiffusion where solute atoms migrate toward the cold side of the ampoule. This behavior

suggests that compositional and interfacial effects dominate under weak thermal driving forces. Near 24°C.cm^{-1}, crosses zero, marking a transition where thermal and concentration-driven fluxes balance. Beyond 24°C.cm^{-1}, becomes negative $S_T < 1$, and increases with gradient, confirming normal thermodiffusion with solute migration toward the hot zone. The observed sign reversal indicates the threshold of thermally controlled segregation, consistent with the detached growth and stabilization of the solute distribution in the $In_{0.5}Ga_{0.5}Sb$ grown crystals by VDS process.

This sign change reflects local inversions in the concentration vs gradient slope (the slope dC/dG crosses zero) Table 6, 7. It is sign where solute migration direction reverses as the possible evidence of interface effects, detachment, or convective changes in the melt. The variation of the Soret coefficient (S_T) across the detached VDS growth region reveals a distinct thermodiffusion-dominated transport mechanism. The measured concentration data indicate that solute transportation is governed by temperature-driven diffusion rather than convective flow. This transition from strong thermodiffusion to quasi-equilibrium confirms that complete ampoule detachment effectively suppresses buoyancy-driven convection, producing a diffusion-controlled environment. Under such conditions, the melt behaves as a quasi-equilibrium solidification system where mass transport occurs by coupled thermal and concentration gradients, validating the diffusion-controlled entire detached growths. Subsequently, the solute redistribution occurs in a diffusion-controlled environment that closely mimics quasi-microgravity. Such behavior is consistent with previous observations in detached InSb and GaSb growth under microgravity and VGF processes [21-36], confirming that the combined influence of thermodiffusion and detachment effectively reproduces the essential effect of low-gravity solidification of the $In_{0.5}Ga_{0.5}Sb$. The non-existence of buoyancy-driven convection within the sealed ampoule confines mass transport to diffusion and thermodiffusion processes.

3.10 Mechanism of detached growth in VDS and Soret effect

In contrast to conventional Bridgman or VGF or Czochroeski techniques, where melt convection and wall contact often induce compositional inhomogeneities, the present VDS configuration provides a mechanically and thermally isolated environment of detachment process in a vertical temperature profile figure 2a:

(a) Region I (G < 20 °C/cm): Positive Soret coefficient at low temperature gradients, atoms (In or Ga) preferentially migrate toward the hot side. This behavior is typically linked with dominance of chemical potential gradients over thermal gradients, crystal-melt interface effects (near the detached region), and the thermodiffusion forces, allowing low convective motion. In this range, the atomic motion is directed by the heat flow and melt composition or interfacial curvature promote the diffusion direction locally.

Table 8 The physcical parameters of the InSb,GaSb and InGaSb grown by VDS process

Sr. No	Physical properties	Symbol	InSb	GaSb	InGaSb x=0.5	Quartz	BN

1	Thermal conduct.	k_L (W/m.K	17.7	21.7	17	2.68	54
2	Specific heat	c_{PL} (J/kg K)	350	250	300	1000	2280
3	Viscosity	μ_L (Pa s)	$4x10^{-3}$	$2x10^{-3}$	$3x10^{-3}$		
4	Thermal diffusivity	α_L (m^2/s)	$2.3x10^{-6}$	$1x10^{-5}$	$9.4x10^{-6}$	$10x10^{-6}$	$8.2x10^{-6}$
5	Kinematic viscosity	ν_L (m^2/s)	$3.5x10^{-7}$	$2.7x10^{-7}$	$1.7x10^{-7}$		
6	Latent heat	L (J/Kg)			$3.1x10^5$		
7	Thermal exp. coeff.	β_T (1/K)	4.5×10^{-6}	7.75×10^{-6}	$1x10^{-4}$		
8	Solutal exp. coeff.	β_C (1/K)	5.47×10^{-6}	$7.7\times10-6$	$1.0\times10-4$		
9	Electric conductivity	σ(S/m)	$9.4x10^5$		$1x10^6$		
10	Melting point	T(K)	985	798	978	1610	2973
11	Density (S)	ρ_S (Kg/m^3)	5610	5780	5600	2200	2280
12	Density (L)	ρ_L (Kg/m^3)	6060	6320	6060		

(b) Region II (20–24 °C/cm): the diffusion direction reverses. This indicates a critical temperature gradient at which D_T (dC/dT) = 0. In this zone, the crystal from the ampoule wall ensures uniform radial heat transfer, minimizes constitutional supercooling, and promotes axial solute uniformity into VDS process. The variation of the Soret coefficient (S_T) with GaSb% composition during detached VDS growth of $In_{0.5}Ga_{0.5}Sb$ is shown in Table 6, 7. The values of Soret coefficient (S_T) were calculated using the experimentally measured thermal gradients and concentration profiles. In VDS process, GaSb% composition gradually increases, $In_{0.5}Ga_{0.5}Sb$ composition decreases, while, GaSb composition approaches near zero at higher gradient, indicating reversal of thermo-diffusion with GaSb transport toward the hot zone. This trend reflects the compositional stabilization of the melt and the transition from diffusion-controlled to equilibrium-controlled growth under steady-state. This condition leads to compositionally enhanced crystallized solidification, where, the entire detached growth into VDS process under quasi-microgravity-like conditions, it marks the transition between reverse and normal thermodiffusion. Physically, this corresponds to the detachment threshold in VDS process, where the melt composition gradient inverts and solute redistribution become purely

temperature-driven.

(c) Region III (G > 24 °C/cm): negative Soret coefficient at higher gradients becomes negative and decreases in magnitude indicating normal thermodiffusion with solute atoms (Ga) moving toward the hot zone. This is the classical Soret effect, the heat flow drives atomic redistribution along the thermal gradient. Diffusion aligns with entropy minimization (atoms transport to higher temperature zones). The magnitude grows with showing stronger coupling between heat and mass transport. Gradient range dominant process, and the physical meaning 12–20 °C/cm positive thermodiffusion in which a melt composition dominates; the solute moves toward cold side at 22 °C/cm zero transition.

The balance of concentration and temperature-driven flux >24°C/cm reversal with negative normal thermodiffusion, the solute migrates toward hot side (stable segregation). Causes of sign change, thermally induced segregation reversal and the Ga species have opposite thermal diffusivities as the gradient increases.

3.11Thermodiffusion and solute redistribution in VDS process

Calculation performed using below equations Table 6, 7, where, the temperature gradient promotes the concentration gradient under diffusion and thermodiffusion coupling:

$$S_T = (1/ C(1-C)) (\nabla C/ \nabla T) \quad (5)$$

Soret coefficient (S_T) evolves across the entire detached growths of $In_{0.5}Ga_{0.5}Sb$ in VDS process from strongly positive at the In-rich initial zone to nearly neutral/negative near the GaSb-rich end, indicating thermal diffusion reversal and compositional stabilization. The variation of the Soret coefficient (S_T) were calculated using the measured thermal gradients and concentration profiles across successive growth zones Table 6, 7. The trend indicates the compositional stabilization of the melt and the transition from diffusion-controlled to equilibrium-controlled growth under steady-state VDS conditions. [30-36]. The influence of thermodiffusion was analyzed for the concentration and temperature gradients along the growth axis. Therefore, the total solute flux is –

$$J = -D\, dC/dz - D_T\, dT/dz \quad (6)$$

where, D: the mass diffusion coefficient, D_T**:** the thermal diffusion coefficient and the Soret coefficient ($S_T = D_T/D$). The counteracts natural segregation, ensuring a more uniform In/Ga ratio across the interface, then in the controlled VDS configuration, solute diffusion becomes a non-linear dynamic process governed by coupled thermal and concentration gradients. Consequently, both the temperature and concentration fields remain individually stable allowing diffusion-dominated growth to proceed under quasi-microgravity conditions. The large axial temperature gradient (~32°C) at the furnace centre enhances thermodiffusion, which dominates solute transport within the sealed ampoule where convection is strongly suppressed. The Soret diffusion coefficient (S_T) quantifies thermally induced solute redistribution [32, 34] in Table 6, 7 calculated using equations:

$$S_T = - (\Delta c / \Delta T) (c_0 / (1 - c_0) \quad (7)$$

$$S_T = 1/C(1-C) (\nabla_C/ \nabla T) \quad (8)$$

where the concentration and temperature differences, respectively showed, and c_0 is the initial solute concentration. The purification factor (PF), the solute redistribution and self-purification, is expressed as:

$$\mathbf{PF = C_0/C_X(1\text{-}f)^{(f\text{-}1)}} \quad (9)$$

where C is the solute concentrations at the melt origin and at a distance 'x', and f is the fraction of crystal solidified. Thermodiffusion coefficient varies non-linearly with temperature [33, 34] by

$$\boldsymbol{D_T = D_0 + \partial D/\partial T\,(T - T_0)}$$

calculated values are Table 6, 7. At steady state, the mass flux balance for the ternary In–Ga–Sb alloy [26, 30, 33] is described as:

$$\mathbf{J = -\rho_0 \sum D\nabla_C - \rho_0 C\,(1 - C)\,D_T\nabla_T} \quad (10)$$

The Soret effect introduces temperature-induced mass diffusion that counterbalances buoyancy flow [34]. This counteraction promotes compositional homogeneity near the crystal-melt interface growth front and contributes to interface stabilization. Thus, by carefully adjusting the thermal gradient, pressure, and ampoule geometry, the Soret-induced diffusion effectively leads to low-convection conditions, uniform growth, defect-free detached growth. This bidirectional counter-flux reduces segregation at the interface and balances solute distribution across the melt. In the detached system, where convection is nearly eliminated, 97% of solute transport arises from thermodiffusion, while only ~3% is attributed to normal Fick's diffusion. The combined effect of the Soret flux and gap width of detachment yields a planar, defect-free interface and improved compositional behaviour ($\Delta x < 0.01$). Axial temperature and solute distribution in the detached VDS growth region of $In_{0.5}Ga_{0.5}Sb$, in which the temperature gradient ($G \approx 10–32°C.cm^{-1}$) drives solute redistribution through thermodiffusion.

3.12 Governing equations of the melt in the VDS process

The melt phase governs the transport of momentum, heat, and solute during crystal growth in the VDS process. In detached growth, the melt is separated from the ampoule wall by a thin gap width or vacuum layer, producing modified boundary conditions and distinct thermocapillary interactions. The melt behaves as an incompressible Newtonian fluid, and its dynamics defines the fundamental conservation equations of mass, momentum, energy, and species transport, at the crystal-melt interface, and the heat and solute balances. These coupled set of equations governs the melt dynamics in the VDS process –

1. Continuity equation:

$$\boldsymbol{\nabla\cdot\vec{v} = 0} \text{ or in general form: } \boldsymbol{\partial\rho/\partial t + \nabla\cdot(\rho\vec{v}) = 0.} \quad (11)$$

Detached growth leads to $v \to 0$, confirming convection-free transport. Ensures conservation of mass in the melt. In crystal growth, the solute solution melt of $In_{0.5}Ga_{0.5}Sb$ the density variation is small, so incompressible approximation is valid, and important for modeling flow circulation, especially near the detached crystal-melt interface. Accordingly, the buoyancy effects disappear due to detachment in VDS process; Marangoni flow is negligible (constant radial $\Delta T \approx 1.4$ °C) wall shear is zero. Thus, $v \approx 0$, and momentum transport becomes diffusion-

dominated.

2. Momentum Conservation (Navier–Stokes equation):

$$\rho(\partial \vec{v}/\partial t+(\vec{v}\cdot\nabla)\,\vec{v}) = -\nabla p+\mu\nabla^2\vec{v}+\rho\vec{g}+\vec{F}\sigma. \quad (12)$$

It governs fluid motion due to thermal, solutal, and capillary (Marangoni) gradients. In detached growth, Marangoni convection along the crystal-melt interface dominates, and Buoyancy term (ρg) becomes weak under quasi-microgravity (low-gravity in VDS process). Since v ≈ 0, heat is transferred mainly by conduction. The axial gradient (10–32°C·cm^{-1}) governs solute redistribution and interface shape.

3. Energy Conservation (Thermal Transport)

$$\rho cp(\partial T/\partial t+\vec{v}\cdot\nabla T) = k\nabla^2 T+Q. \quad (13)$$

This equation describes heat transfer by conduction, convection, and sometimes radiation. Determines temperature gradients that drive thermocapillary (Marangoni) flow and Soret (thermodiffusion) effects and controlling interface shape and stability during detached crystal growth by VDS process.

4. Species (Mass Transport) Equation

$$\partial C_i/\partial t+\vec{v}\cdot\nabla C_i = D_i\nabla^2 C_i+D_{Ti}\nabla^2 T. \quad (14)$$

It describes solute redistribution in the melt, the diffusion coefficient D_i and the thermal diffusion coefficient D_{Ti} of i^{th} species, and the term $\nabla^2 T$ represents the Soret effect. In VDS, v ≈ 0 → convection term vanishes → thermodiffusion dominates $\nabla^2 T$ couples temperature gradient to composition gradient, which is important for In–Ga–Sb alloy systems, and predicting detached growth stability and composition uniformity. The interaction between thermal, solutal, and capillary forces dictates convection patterns, interface morphology, and detachment stability. In VDS process, the proper control of these parameters allows simulation leading to uniform composition and smooth interface growth of InSb, $In_{0.5}Ga_{0.5}Sb$, GaSb phases by entire detached crystals. Coupling under detached growth and detachment enforces, there is no-slip melt, thus, wall boundary condition removed stable temperature field, 1D diffusive solute field has a thin diffusion layer (δ ~ 0.5–3 mm). Thus, melt transport is controlled by diffusion and thermodiffusion, producing enhanced crystal growth.

3.13 The Mullins–Sekera stability criterion

The Mullins–Sekerka (MS) theory provides a condition for stability of interfaces, wherein, the phase transformation grow during growth by the phase separation at sufficient boundary conditions due to the temperature and its gradients in directional crystallization of a binary / ternary melt, is the principle of the morphological stability by Mullins-Sekerka [J. Appl. Phys. **1964**, 35, 444]. However, the boundary conditions have dependent on the predetermined distance from the solidification front for providing directional solidification, where, it distresses the rate of perturbations by intensification in the crystal-melt interface - i) the effect of distance from solidification front, where the cooling zone influences both the thermal and concentration gradients and ii) the gradients define the front velocity, where intensification rate

of perturbations depend on the distance between cooling zone and solidification front, which perturb the stability in growing solidification front.

The equivalence between VDS growth and quasi-equilibrium solidification was verified through the hydrodynamic, [9-12, 18-20] thermodiffusion, [30-36] and Mullins–Sekerka (MS) interface stability, [36] and the melt governing equations. [21-29]. Dimensionless parameters confirmed that buoyant convection was negligible (Gr ≪ 1, Pe ≪ 1). The Mullins–Sekerka criterion for planar-interface stability requires:

$$\text{I)} \quad \mathbf{G/V > m\,C_0(1-k)/\,kD} \tag{15}$$

$$\text{II)} \quad \mathbf{Vc = G\,k\,D/\,m\,C_0(1-k)} \tag{16}$$

Where G = thermal gradient, V = interface velocity, m = liquidus slope, C_0 = initial solute concentration, k = partition coefficient.

Using VDS process experimental data (m = 6000 °C, k = 0.5, C_0 = 0.3, D = 2 × 10^{-5} cm^2 s^{-1}), the critical growth velocity (Vc) was estimated as 4 × 10^{-4} to 8 × 10^{-4} m s^{-1}. The experimental growth rate V (3 × 10^{-3} m s^{-1}) satisfied, confirming that the detached interface remained planar (V >Vc) and stable throughout solidification. This result validates that the VDS system satisfies hydrodynamic, thermodynamic, and the quasi-microgravity equivalent conditions, reproducing diffusion–capillary-controlled crystal growth. Because V > Vc, the MS stability condition is satisfied, ensuring the planar interface, hence no cellular/dendritic breakdown in entire detached growth by VDS process, stable solute boundary layer was absence of striations. Experimental interface shapes (concave → planar → convex) correspond precisely to MS predictions combined with thermodiffusive polarity. Detached VDS growth therefore meets all thermodynamic and hydrodynamic conditions for stable planar solidification.

3.14 Gravity–diffusion number (GD) as a stability criterion

A new dimensionless number for VDS growth process, the Gravity–Diffusion Number (GD) was introduced to quantify the competition between gravitational convection, viscous diffusion, and capillary stabilization. This GD quantifies the relative importance of gravitational (buoyancy-driven) transport compared to diffusive and viscous resistances in the melt, modified by the strength of thermal and solutal gradients. It predicts the stability, and completion of entire detached growth. As temperature increases, GD decreases shifting control from gravitational convection to capillary–diffusion stabilization — the essential mechanism for entire detached growth under quasi-equilibrium solidification conditions. It is proposed to quantify the balance between gravitational convection, and capillary stabilization in the VDS process during entire detached crystal growth. It represents thermal solutal coupling. GD quantifies the competition between buoyancy and diffusion–capillary stabilization at the crystal-melt interface, and it is defined:

$$\mathbf{G_D = \rho g R^2 D\mu\,/\,f(\Delta T, \partial c/\partial z)} \tag{17}$$

Where, the melt density (ρ), gravitational acceleration (g), ampoule radius (R), diffusion coefficient (D), viscosity (μ), temperature difference (ΔT), concentration gradient ($\partial c/\partial z$) and the f (ΔT, $\partial C/\partial z$) is the thermal–solutal driving function, see Table 6-8 and reported data of VDS process [37-51]. High GD values correspond to gravity-dominated regimes (partial

detachment), while low GD values indicate diffusion–capillary control and entire detachment. Experimental observations demonstrated that as temperature increased, GD decreased, signifying a transition from buoyancy-driven to diffusion-capillary-controlled growth. It is predicted that at sufficiently low GD, the melt behaves as in true quasi-microgravity, producing planar detached interfaces and uniform, defect-free crystals. This condition was satisfied by entire detached growth in VDS process. Thus, GD serves as a unified parameter linking gravitational suppression, diffusion kinetics, and interface stability. Temperature dependence experimental data show GD decreases monotonically with temperature, indicating the buoyancy effects is weaken; thus, the diffusion dominates thermodiffusion controls segregation interface satisfies Mullins–Sekerka conditions. GD correlates strongly with Soret polarity reversal, In-rich to Ga-rich composition transitions, stable gap width thickness. GD provides a unified measure linking with gravitational suppression, diffusion–thermodiffusion control interface stability and entire detached growth behavior. This study reveals the complete detachment of the crystal from the ampoule wall was maintained throughout growth. Convection was effectively suppressed, achieving quasi-equilibrium solidification. The Soret effect governed solute redistribution, yielding uniform In–Ga–Sb alloy composition. The Mullins–Sekerka criterion confirmed diffusion-capillary-controlled planar interfaces. The Gravity–Diffusion number provided a quantitative measure of entire detachment stability.

3.15 Mechanism of Entirely Detached Growth

The entirely detached growth mechanism in the VDS process is governed by the combined effects of:

- Thermal gradient–induced diffusion
- Thermodiffusion effect
- Capillary forces and vapor pressure
- Suppression of convection

The narrow gap formed between the crystal and ampoule wall acts as a thermal buffer, minimizing shear stress and lateral heat transfer. This configuration enables a stable, planar interface and diffusion-controlled solidification.

Consequently, the system behaves as a quasi-microgravity environment, where mass transport is dominated by diffusion rather than convection.

Conclusion

This work establishes a diffusion-controlled mechanism for the entirely detached growth of $In_{0.5}Ga_{0.5}Sb$ crystals using the VDS process under terrestrial conditions. The introduction of a controlled gap between the crystal and ampoule wall effectively suppresses buoyancy-driven convection and creates a quasi-microgravity environment, enabling transport dominated by diffusion and thermodiffusion.

The experimental results demonstrate that stable growth is achieved under axial temperature gradients of 10–32 $°C \cdot cm^{-1}$ and low translation rates, satisfying the constitutional supercooling criterion and maintaining a planar crystal–melt interface. The coupled action of Fickian

diffusion and Soret-driven thermodiffusion governs solute redistribution, resulting in compositional uniformity and polarity reversal near equiatomic composition.

Dimensionless analysis (Pe ≪ 1, controlled Rayleigh number) confirms that convective effects are negligible and that mass transport is diffusion-dominated. The evaluated Soret coefficient reveals a transition from positive to negative values, indicating thermodiffusion reversal and compositional stabilization along the growth axis.

Characterization results, including XRD, FTIR, Raman spectroscopy, Hall measurements, and microhardness analysis, confirm enhanced crystalline quality, reduced defect density, and improved electrical performance compared to conventional growth techniques. The absence of growth striations and microbanding further validates the stability of the detached interface.

Overall, the VDS process provides a dynamic and scalable terrestrial approach for achieving quasi-equilibrium solidification conditions analogous to microgravity. The proposed diffusion-controlled framework and detached growth mechanism offer a significant advancement in the growth of ternary III–V semiconductor crystals, particularly for applications requiring high compositional uniformity and defect-free structures.

Acknowledgements

The author expresses sincere gratitude to Prof. B. M. Arora for his valuable guidance and scientific support. The author also thanks Dr. Shilpa Kalantre for continuous encouragement, Ms. Snehal Gadkari for computational assistance, and Mrs. Sarojini Gadkari for her constant motivation throughout this work.

Author Contribution: All conceptualization, experimental work, analysis, modeling, interpretation, and manuscript preparation were carried out solely by the author.

Competing Interest: The author declares no competing interests.

Funding: This work received no external funding.

Conflict of Interest: The author declares no conflict of interest.

Data Availability: All data supporting this study are included in the manuscript.

References

[1] T. J. Bright, L. Wang, Z. M. Zhang, *J. Heat Transfer 136,* 2014, 062701.

[2] G. B. Stringfellow, *J. Phys. Chem. Solids 33,* 1972, 665.

[3] Y. Wang, L. L. Regel, W. R. Wilcox, *J. Cryst. Growth* 209, 2000, 175.

[4] Y. Wang, L. L. Regel, Wilcox, *J. Cryst.* Growth *243*, 2002, 546.

[5] J. B. Wang, L. L. Regel, Wilcox, *J. Cryst. Growth 260,* 2001, 590.

[6] T. Duffar, P. Dusserre, N. Giacometti, *J. Cryst. Growth 223,* 2004, 69.

[7] M. Fiederle, T. Duffar, V. Babentsov, K. W. Benz, P. Dusserre, *Cryst. Res. Technol. 39,* 2004, 481.

[8] S. Balinta, L. Braescua, L. Syllab, S. Epurea, T. Duffar, *J. Cryst. Growth 310*, 2008, 1564.

[9] C. Stelian, A. Yeckel, J. J, Derby, *J. Cryst.* Growth 311*,* 2009, 2572.

[10] A.Yeckel, J. J. Derby, J. *Cryst. Growth 314,* 2011, 310

[11] A. Yeckel, P. Daoutidis, J. J. Derby, *J. Cryst. Growth 356*, 2012, 33.

[12] A. Yeckel, P. Daoutidis, J. J.Derby, *J. Cryst. Growth* 361, 2012, 16.

[13] A. J. Goza, S. E. Tritchler, B. C. Houchens, *J. Cryst. Growth* 337, 2011, 60.

[14] A. E. Voloshin, A. A. Lomov, P. Ge, C. Huo, *J. Cryst. Growth 236*, 2002, 501.

[15] A. E. Voloshin A. E., T. Nishinaga, P. Ge, C. Huo, *J. Cryst. Growth* 234, 2002, 12.

[16] V. Strelov, I. Kuranova, B. G. Zakharov, A. E. Voloshin, *Crystallography. Rep 59,* 2014, 781.

[17] Y. A. Serebryakova, V. N. Vlasova, V. S. Sidorova, *J. Surf. Inve. Synchr. Neut. Tech*. 6, 2012, 604.

[18] P. Rudolph, *AIP Conf. Proc. 1270*, 2010, 107.

[19] P. Rudolph, M. Czupalla, B. Lux, *J. Cryst. Growth* 311, 2009, 4543.

[20] L. Gránásy, G. I. Tóth, J. A. Warren, F. Podmaniczky, Tegze, *Prog. Mater. Sci*. 106, 2019, 100569.

[21] J. Yu., Y. Inatomi, V. Kumar, Y. Hayakawa, Y.Okano, Y Momose, npj Microgravity 5, 2019, 1.

[22] X. Jin, B. Wang, *J. Cryst. Growth 607*, 2023, 127110.

[23] N. Bergeon, G. Reinhart, F. L. Mota, H. Nguyen, *Flowing Matter*, *44,* 202198.

[24] M. N. Takagi, Y. Hayakawa, S. Dost, *J. Cryst. Growth 385,* 2014, 66.

[25] Ghritli R., Okano Y., Inatomi Y., Dost S., J. Cryst. Growth *573*, 2021, 126280.

[26] Ghritli R., Okano Y., Inatomi Y., Dost S., Jpn. *J. Appl. Phys. 61*, 2022, 115502.

[27] Ghritli R., Okano Y., Inatomi Y., Dost S., J. Chem. Eng. Jpn56, 2023, 2222757.

[28] Y. Hayakawa, T. Koyama, Y. Momose, Y. Inatomi, *Int. J. Microg Sci. Appl. 34,* 32017, 40111.

[29] M. A. Rahman, M. Z. Saghir, *Int. J. Heat Mass Transf.* 73, 2014, 693.

[30] D. V. Alexandrov, D. L. Aseem, *Comput. Mater. Sci. 37,* 2006, 1.

[31] M. F. Mangler, M. C. Humphreys, E. Geifman, A. A. Iveson, A. Lindoo, *J. Petrol. 64,* 2023, 54.

[32] X. Liu, H. Fan, Y. Shan, *PLoS ONE 19,* 2024, e0313150.

[33] P. Costesèque, A. Mojtabi, J. K. Platten, *Comptes Rendus Mécanique*, *339,* 2011, 275.

[34] Xiaoxia Liu, Hailong Fan, Yanyan Shan, *PLoS ONE 19*, 2024, e0313150.

[35] Morteza Eslamian , M. Ziad, Saghir Show, *Intern J Therm Sci, 50*, 2011, 232.

[36] Dmitri V. Alexandrov, Peter K. Galenko, *J. Appl. Phys., 136,* 2024, 055103

[37] D. B. Gadkari, B. M. Arora, *Trans. Mater. Soc. Jpn., 34,* 2009, 571.

[38] D. B. Gadkari, *J. Chem. Chem. Eng. 6,* 2012, 65.

[39] D. B. Gadkari, *J. Chem. Chem. Eng. 6,* 2012, 258.

[40] D. B. Gadkari, *J. Mater. Sci. Eng. A*, 2, 2012, 593.

[41] D. B. Gadkari, *AIP Conf. Proc. 1512,* 2013, 856.

[42] D. B. Gadkari*, J. Mater. Sci. Eng. A 3,* 2013, 338, .

[43] D. B. Gadkari, B. M. Arora, *Mater. Chem. Phys. 139*, 2013, 375.

[44] D. B. Gadkari, *Int. J. Sci. Res. Publ. 4,* 2014, 1.

[45] D. B. Gadkari, *Int. J. Eng. Res. Appl. 2,* 2015, 39.

[46] D. B. Gadkari, D. Maske, M. Deshpande, B. M. Arora *IJIRSET 5,* 2016, 20925.

[47] D. B. Gadkari, *Int. J. Eng. Res. Appl. 9*, 2019, 1.

[48] D. Maske, M. Deshpande, D. B.Gadkari, *J. Nano Electron. Phys. 12,* 2020, 2012.

[49] D. B. Gadkari, *Int. J. Eng. Res. Appl 10,* 2020, 5.

[50] D. B. Gadkari, *Int. J. Eng. Res. Appl. 10,* 2020, 35.

[51] D. B. Gadkari*, Int. J. Eng. Res. Appl. 10,* 2020, 7.